Journal of Photochemistry and Photobiology A: Chemistry 203 (2009) 64–71

Contents lists available at ScienceDirect

Journal of Photochemistry and Photobiology A: Chemistry

journal homepage: www.elsevier.com/locate/jphotochem

Effect of Fe^{3+} ion doping to TiO_2 on the photocatalytic degradation of Malachite Green dye under UV and vis-irradiation

Meltem Asiltürk[a,*], Funda Sayılkan[a], Ertuğrul Arpaç[b]

[a] Prof. Dr. Hikmet Sayılkan Research and Development Laboratory for Advanced Materials, İnönü University, 44280 Malatya, Turkey
[b] Akdeniz University, Faculty of Arts and Science, Department of Chemistry, 07100 Antalya, Turkey

ARTICLE INFO

Article history:
Received 6 October 2008
Received in revised form 16 December 2008
Accepted 17 December 2008
Available online 25 December 2008

Keywords:
TiO_2
Fe^{3+}-doping
Thin film
Photocatalysis
Degradation

ABSTRACT

Fe^{3+} ion-doped TiO_2 particles were synthesized by the hydrothermal process at 225 °C. Titanium isopropoxide ($Ti(OPr^i)_4$) was used as precursor material. Both undoped and doped TiO_2 particles were used to coat glass surface. The coated surface was examined with respect to their photocatalytic performance for degradation of Malachite Green (MG) dye in aqueous solution under UV and vis-light irradiation. The particles and the films were characterized by XRD, SEM and UV/vis/NIR techniques. The results showed that crystallite size of the hydrothermally synthesized TiO_2 particles are in nanoscale. Anatase was only the crystalline phase. Doping of Fe^{3+} ion improved the photodegradation performance of TiO_2 coated surfaces. Degradation performance of Fe^{3+} doped TiO_2 coated surfaces determined under UV- and vis-irradiation conditions was higher than the undoped TiO_2 coated surface. It was concluded that the photodegradation of 2.5 mg L^{-1} MG under UV-light irradiation with the catalysis of Fe^{3+}-doped TiO_2 follows the pseudo-first-order reaction kinetics with the rate constant of 0.0202 min^{-1}.

1. Introduction

If the literature is anything to go by, semiconductor photochemistry continues to be the hottest subject in photochemistry. Recently, greatest interest in the subject has focused primarily on the semiconductor photocatalysis (SPC) as a possible route for providing clean water, air and surfaces [1–3]. The basic process for SPC is summarized as

$$\text{organic pollutant} + O_2 \xrightarrow[\text{semiconductor}]{h\upsilon \geq E_{bg}} CO_2 + H_2O + \text{minerals}$$

where minerals are generated if there are any hetero atoms such as S, N and Cl, present in the original organic pollutant. Here, E_{bg} is the band gap energy of the semiconductor. As a popular photocatalyst, anatase titanium dioxide has been widely studied because of its various merits, such as chemical and biological inertness, mechanical toughness, excellent photocatalytic activity, low cost and easy of deposition [4,5]. The synthesis of TiO_2 has attracted extensive attention due to its effective photodegradation activity for organic pollutants in water and air under illumination of UV-light [6–8]. Recently, most of the investigations have focused on preparing TiO_2 catalysts which can be activated by VIS-light because there is much more energy produced by the sunlight in the visible lights region compared to the UV region [9–11]. Generally, doping or combining of TiO_2 with various metal or non-metal ions was reported as a good tool to improve the photocatalytic properties [12,13] and for enhancement of visible light response [14]. Metal ion dopants may act as electron or hole traps and, consequently, alter electron-hole pair recombination rates. Indeed, special efforts have been dedicated to doping TiO_2 with Fe^{3+} ions [15–17]. Amongst a variety of transitional metals, iron has been considered to be an appropriate candidate due to the fact that the radius of Fe^{3+} (0.79 Å) is similar to that of Ti^{4+} (0.75 Å), so that Fe^{3+} can be easily incorporated into the crystal lattice of TiO_2 [18]. This interest is based on the idea that Fe^{3+} ions act as shallow charge traps in the TiO_2 lattice [18–20]. However, the role of Fe ions in TiO_2 is controversial. Some authors suggest the Fe^{3+} behaves as $\bar{e}/h^+$ recombination center [21]. Other authors have postulated that the role of dopant ion is to favor $\bar{e}/h^+$ separation, which enhances the photoactivity [15,16,18,22].

Due to the large number of possible variations, it is rather difficult to find out the appropriate compositions and concentrations of dopants, especially if lattice doping should be avoided. For these reasons, it is likely that investigations will continue for many years to find suitable and efficient photocatalysts to function under daylight conditions.

Up to now, many methods such as the sol–gel process [23–26], metal organic chemical vapor deposition (MOCVD) [27,28], the microemulsion or the reverse micelles and the hydrothermal process have been established for the synthesis of TiO_2 catalysts. However, above methods, except for the hydrothermal process, have some disadvantages for industrial applications. For example, the sol–gel process is more common but needs high temperature

* Corresponding author. Tel.: +90 422 341 0010.
E-mail address: masilturk@inonu.edu.tr (M. Asiltürk).

1010-6030/$ – see front matter © 2008 Elsevier B.V. All rights reserved.
doi:10.1016/j.jphotochem.2008.12.021

(>500 °C) for obtaining TiO_2 crystalline particles. TiO_2 nanoparticles synthesized by the hydrothermal process have some typical properties, such as being in pure anatase crystalline phase, having fine size with more uniform distribution, high-dispersion ability either in polar or non-polar solvents, easy coating on different supporting material since TiO_2 particles disperse in various solvent system [29]. It is well known that the photocatalytic performances of TiO_2-based thin films depend strongly on the methods of metal ion doping and the amount of doping, since they give a decisive influence on the properties of TiO_2 thin film [30–32]. Therefore, it is necessary to investigate the effects of doping method and doping content on the photocatalytic performance of TiO_2-based thin films.

In this work, Fe^{3+}–TiO_2 particles were hydrothermally synthesized at 225 °C. Photocatalytic activity of Fe^{3+} doped and undoped TiO_2 thin films supported on glass were examined for the degradation of Malachite Green in aqueous solutions under UV and vis-lights.

2. Experimental

2.1. Chemicals and apparatus

As the starting precursors, the following reagents were employed: titanium-(IV)-isopropoxide, [$Ti(OPr^i)_4$, Alfa Aesar, 97%], as TiO_2 source; hydrochloride acid (HCl, Merck, 37%) as catalyst; Iron(III) nitrate [$Fe(NO_3)_3{\cdot}9H_2O$, Alfa Aesar, 99%] as dopant source; deionized water as hydrolysis agent; 3-glycidoxypropyltrimethoxysilane (GLYMO, Aldrich, 98%) and tetraethylorthosilicate (TEOS, Aldrich, 98%) as binder reagents; 2-butoxyethanol (2-BuOEtOH, Aldrich, 99%), ethyl alcohol (EtOH, 96%), and n-propanol (98%) as solvents. Oxalate salt of Malachite Green ($[(C_{23}H_{25}N_2)(C_2HO_4)]_2{\cdot}C_2H_2O_4$) (MG) used as the model pollutant and purchased from a local textile factory was of analytical reagent grade.

Berghoff model hydrothermal unit interfaced with a temperature controller (up to 250 °C) and timer unit was used for the synthesis of TiO_2. In order to determine the crystal phases in the powder samples, Rigaku Geigerflex D Max/B MGdel X-ray diffractometer (XRD) with Cu Kα radiation (λ = 0.15418 nm) in the region $2\theta = 10–70^\circ$ with a step size of 0.04° was used. The average crystallite size of the particles were calculated according to the following Scherrer's equation,

$$d_{hkl} = \frac{k\lambda}{(\beta\cos(2\theta))} \quad (2)$$

where d_{hkl} is the average crystallite size (nm), λ is the wavelength of the Cu Kα radiation applied (λ = 0.154056 nm), θ is the Bragg's angle of diffraction, β is the full-width at half maximum intensity of the peak observed at $2\theta = 25.24$ (converted to radian) and k is a constant usually applied as ∼0.9.

The Brunauer–Emmett–Teller (BET) surface area, average pore diameter and micropore volume of the TiO_2 particles were analyzed by nitrogen adsorption using Asap 2000 model BET analyzer. During the BET analysis, the samples were degassed at 130 °C for 4 h prior to nitrogen adsorption measurements. The BET surface area was determined by multipoint BET method using adsorption data in the relative pressure (P/P_o) range of 0.02–0.3. Surface morphologies of the particles and coated surfaces were investigated using LEO Evo 40 model scanning electron microscope (SEM). The amount of iron in Fe^{3+} doped TiO_2 was determined by PerkinElmer, Analyst 800 model flame atomic absorption spectrometer (FAAS) in the centrifuged solution obtained after the hydrothermal treatment. Contact angles of coatings with water were measured by Rame Hart 100–00 model goniometer. Film thickness of the coated surfaces was measured by Mahr-M1 model perthometer. For this purpose, half of the glass plate area was coated. Film thickness was automatically measured from the thickness differences between coated and uncoated surfaces sides.

Dye concentration in the aqueous solution was measured by Varian Carry 5000 model UV–vis-NIR spectrophotometer. Coated surfaces positioned in the dye solution were irradiated with and without 400 nm cut-off filter without shaking in a Solar Box 1500 model radiation unit combined with a Xe-lamp (690 W m^{-2}) and operated with a controller for timing and power input between 390 and 1100 W m^{-2}.

2.2. TiO_2 synthesis

The method employed for the synthesis of TiO_2 in this work is similar to that reported elsewhere [33], which employs a hydrothermal process in which $Ti(OPr^i)_4$ was used as starting material. 11 mL of 97% $Ti(OPr^i)_4$ solution was dissolved in 32 mL of 98% n-propanol. After stirring for a few minute at room temperature, 0.587 mL of 0.1N HCl was drop wise added to the above alkoxide solution with a burette under stirring conditions. Then, 0.042 and 1.016 g of ferric nitrate was suddenly added in order to obtain $Fe^{3+}/Ti(OPr^i)_4$ ratios (mol/mol) as to be 0.003 and 0.07, respectively. The last solution was stirred until a clear and homogeneous solution with slightly brown and dark brown color formed. A mixed solution of 0.831 mL water for 0.003 $Fe^{3+}/Ti(OPr^i)_4$ ratio or 0.424 mL water for 0.07 $Fe^{3+}/Ti(OPr^i)_4$ ratio and 5 mL of 98% n-propanol was added dropwise to the last solution by burette under stirring. The reaction was allowed to continue for 1 h, and sol–solution was transferred into a 250 mL Teflon crucible, then left in a pre-heated (225 °C) stainless steel autoclave device. The reaction was allowed to occur at 225 °C for 1 h. After this time, autoclave was removed from the heating unit and cooled down to room temperature. As-obtained powders were separated through centrifuging and dried in a vacuum sterilizer. Thus, primrose yellow and cream TiO_2 particles were obtained. Undoped TiO_2 ($UTiO_2$) with a white color was also synthesized as described above, with the exception of using dopant. $HCl/Ti(OPr^i)_4$, and $H_2O/Ti(OPr^i)_4$ ratios (mol/mol) were 0.2 and 2, respectively. In the text, the powders with 0.003 and 0.07 (mol/mol) $Fe^{3+}/Ti(OPr^i)_4$ ratios were described as $0.3FeTiO_2$ and $7FeTiO_2$, respectively.

2.3. Preparation of the coating solution

Prior to preparation of the coating solution, TiO_2 sol was prepared by dispersing TiO_2 in deionized water in the absence of dispersant. This mixture was treated in an ultrasonic bath for a few minutes until transparent TiO_2 sol occurred.

For preparing the coating solution, GLYMO was first reacted with TEOS for 10 min (GLYMO/TEOS: 1, mol/mol), then EtOH was added to this mixture (EtOH/GLYMO: 10.3, mol/mol) and stirred for 10 min. HCl was allowed to react with GLYMO/TEOS/EtOH for 10 min (HCl/GLYMO: 0.055, mol/mol) and finally H_2O was added to GLYMO/TEOS/EtOH/HCl and allowed to react for 10 min (H_2O/GLYMO: 6.5, mol/mol). As a result, the coating solution was prepared. Equivalent weight of TiO_2 sol and the coating solution was mixed and the mixture was stirred for 5 min before adding 2-BuOEtOH. After stirring the mixture for 40 h, transparent coating solution was obtained. Glass surfaces (5 cm × 5 cm) were coated with the coating solution by means of spin-coating apparatus which was operated at 1000 rpm for 10 s. The coated glass surface was treated at 80 °C for 60 min for curing. To be able to maintain a hydrophilic surface, the coated glass surfaces were irradiated under UV lamp operating at 8 W.

2.4. Photocatalytic degradation tests

Photocatalytic performance of the films was examined using the degradation of Malachite Green dye in water. The photocatalytic

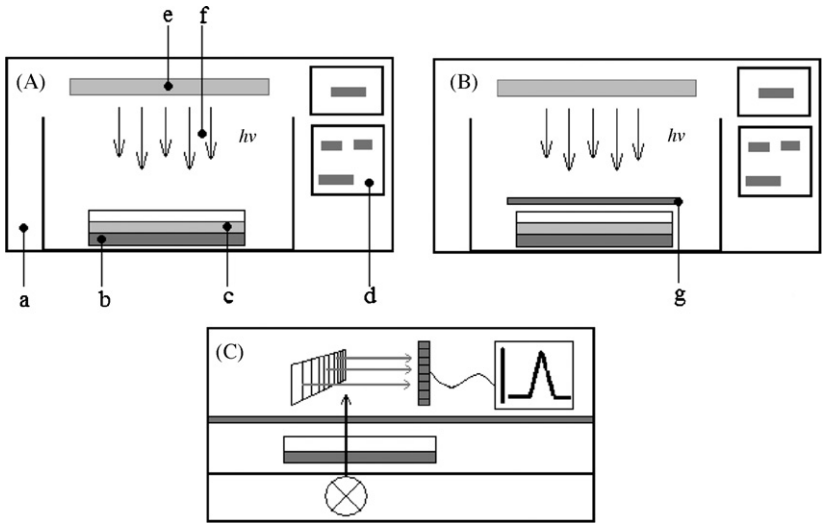

Scheme 1. Photoreactor system. (A) UV irradiation applied without filter, (B) vis irradiation applied with UV cut-off filter, (C) UV measurement after irradiation. (a) Solar Box irradiation unit, (b) Sn doped TiO_2 coated glass plate, (c) dye solution, (d) control unit of the Solar Box, (e) UV lamp, (f) UV lights and (g) Glass UV filter.

degradation intermediates of MG were not determined quantitatively, but the photocatalytic mechanisms of Fe^{3+}-doped TiO_2 particles were tentatively discussed. The coated glass plates were immersed into 25 mL aqueous MG solution at two different concentrations (2.5 and 5.0 mg L^{-1}) in a polystyrene reaction cell which has 12 separate sample compartments and one cover. The cell was immediately located in the Solar Box ready for UV-irradiation. The coated plate and dye solution system was irradiated in the vertical direction without shaking. The distance between the UV lamp and plate/dye solution system was kept within 20 cm. The change of MG concentration with respect to irradiation time was measured by UV/vis/NIR spectrophotometer. The photocatalytic performance was determined without cut-off filter for UV irradiation, and with 400 nm cut-off filter for vis irradiation. The photocatalytic reactor system used for testing the photocatalytic performance of Fe doped and undoped TiO_2 coated surfaces is shown in Scheme 1.

3. Results and discussion

For determining the amount of iron in the precipitated TiO_2 powders, FAAS analysis was performed using the supernatant of TiO_2 containing suspension in the autoclave. It was calculated that the amount of iron in the powder is 0.19 and 4.89 wt.% for $0.3FeTiO_2$ and $7FeTiO_2$, respectively.

XRD patterns of the hydrothermally synthesized TiO_2 particles are shown in Fig. 1. When the patterns were compared with PDF#21-1272 data files, it was found that all peaks observed at 25.16°, 37.91°, 48.19°, 55.01°, 62.68° for $UTiO_2$, and 25.08°, 37.72°, 47.81°, 54.14°, 62.56° for $0.3FeTiO_2$, and 25.20°, 37.62°, 47.88°, 54.32°, 62.61° for $7FeTiO_2$ 2Theta values are consistent with anatase (1 0 1), (0 0 4), (2 0 0), (2 1 1) and (2 0 4) spacings, respectively. Other crystalline forms of TiO_2, namely rutile and brookite, were not detected. Moreover, no other crystalline phases correspond to iron containing compounds were detected in the XRD patterns of $0.3FeTiO_2$ and $7FeTiO_2$. This may be due to the fact that Fe^{3+} ions may substitute Ti^{4+} ions and insert into the crystal lattice of TiO_2, since the radii of Ti^{4+} and Fe^{3+} ions are similar. For a coordination number of 6, Fe^{3+} and Ti^{4+} have similar ionic radius (0.79 Å versus 0.75 Å), so it can be inferred that iron ions might insert into the structure of TiO_2 and located at interstices or occupied some of the lattice sites of TiO_2, forming an iron–titanium solid solution [34]. These results support that the current doping procedure allows uniform distribution of the dopants to form solid solution.

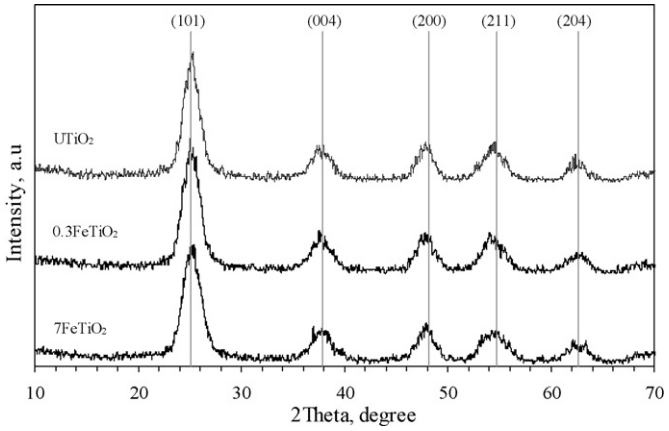

Fig. 1. XRD patterns of $UTiO_2$, $0.3FeTiO_2$ and $7FeTiO_2$ particles.

In order to detect free or segregated iron oxide phase found with Fe^{3+} doped TiO_2 powders, if any, samples of $UTiO_2$, $0.3FeTiO_2$ and $7FeTiO_2$ were heated at 800 °C in air for 2 h and then, heated samples were analyzed by XRD (Fig. 2). The first thing observed from the XRD patterns, all of the peaks of all samples are very sharp and the samples contains very well-formed TiO_2 crystals, as compared to

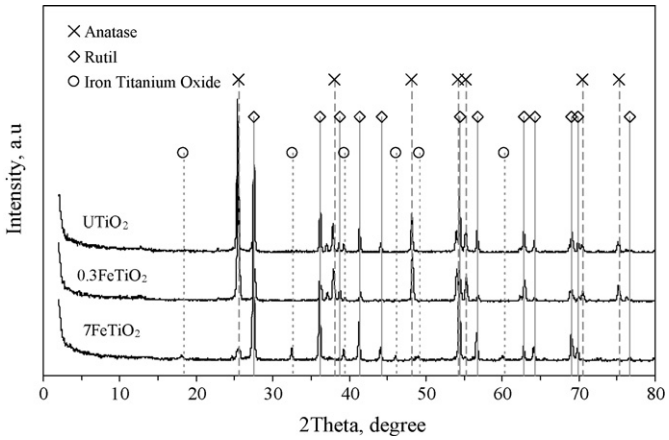

Fig. 2. XRD patterns for the samples of $UTiO_2$, $0.3FeTiO_2$ and $7FeTiO_2$ heated at 800 °C for 2 h.

Table 1
Some intrinsic properties of $UTiO_2$, $0.3FeTiO_2$ and $7FeTiO_2$ particles and films.

	$UTiO_2$	$0.3FeTiO_2$	$7FeTiO_2$
Particle property			
Crystalline type	Anatase	Anatase	Anatase
Particle color	White	Primrose yellow	Dark cream
Crystallite size (nm)	9.76	9.20	9.00
BET surface area ($m^2\ g^{-1}$)	40.84	83	126.1
Film property			
Thickness (μm)	5	6–8	5–7
Contact angle with water (before/after irradiation)	60°/17°	69°/8°	65°/7–8°

the unheated samples (Fig. 1). XRD patterns of $UTiO_2$ and $0.3FeTiO_2$ samples are almost identical and contain both the anatase and rutil phase of TiO_2. It is known that transformation from anatase to rutil phase of TiO_2 occurs in a temperature interval of 700–900 °C. In addition to rutil phase of TiO_2, $7FeTiO_2$ contains also Fe_2TiO_5 as perovskite. Deficiency of Fe_2TiO_5 in the heated $0.3FeTiO_2$ and occurrence in the heated $7FeTiO_2$ was attributed to the occurrence of free iron oxide phase in the unheated $7FeTiO_2$. It was interesting to observe that some of the XRD peaks of anatase in the heated $7FeTiO_2$ either decrease or disappear, while those of rutil stand still and increase. It can be concluded from this experiment that almost all of the Fe^{3+} in $0.3FeTiO_2$ are trapped in the crystal lattice of TiO_2, whereas $7FeTiO_2$ contains segregated iron oxide in addition to Fe^{3+} doped TiO_2.

These results are in good agreement with those observed by Adán et al. [35] suggesting a solubility limit for iron in the anatase structure around 1 wt.%, due to the lattice expansion resulting from compensating effects between iron substitution of titanium cations (Fe^{3+} showing slightly lower ionic radius than Ti^{4+}) and oxygen vacancy formation for maintenance of charge neutrality. However, Fe doping has an effect on the crystallization on TiO_2. It can be seen that the larger amount of Fe doped, the wider the width of diffraction peaks, the worse the crystallization of TiO_2, and the smaller crystallite size calculated from the Scherrer equation of TiO_2 particles. For example, $UTiO_2$ has the crystallite size of 9.80 nm; it decreases to 9.20 and 9.0 nm for $0.3FeTiO_2$ and $7FeTiO_2$, respectively (Table 1). This modification may prevent particle agglomeration, forming well-defined nanocrystalline particles with high surface area [36]. BET surface areas of all particles are shown in Table 1. Reduction in the particle size caused by doping Fe^{3+} ion led to larger surface area. $0.3FeTiO_2$ and $7FeTiO_2$ have high surface areas of 83 and 126.1 $m^2\ g^{-1}$, respectively, while the $UTiO_2$ has very low BET surface area as 41 $m^2\ g^{-1}$. Higher surface area may be benefit to their high photocatalytic performance, due to enhanced adsorption of photons and dye molecules.

Some physicochemical characteristics of the $UTiO_2$, $0.3FeTiO_2$ and $7FeTiO_2$ particles and films are shown in Table 1. The particles have different color changing from white to dark cream. This change was affected by the amount of the Fe addition. As the iron ratio increased as 0.003 (mol/mol) or 0.19 wt.%, the promise yellow color occurs, but further addition of Fe changed the powder color to a dark cream. It is likely that the white $UTiO_2$ powder changed to dark cream due to red shift by the high Fe addition. This result is consistent with UV measurements (Fig. 3).

Diffuse reflectance spectra (DRS) technique is a useful technique to characterize the optical absorption properties of nanoparticles. The DRS spectra of Fe-doped TiO_2 with different modification level in comparison with undoped TiO_2 are shown in Fig. 3. For $UTiO_2$, an absorption edge rising steeply toward the UV below 387 nm can be attributed to band-gap excitation of anatase (~3.2 eV). $UTiO_2$ has no absorption in visible region (>400 nm), whereas Fe-doped TiO_2 samples exhibit red shifts of absorption edge and significant enhancement of light absorption at 400–600 nm. The light absorption in the range from 450 to 650 nm increases with increasing Fe content in TiO_2, accompanied with the changes on color from white to primrose yellow and dark cream. According to the previous reports [23,36], the presence of metal ions in TiO_2 does not modify the position of the valence band edge of TiO_2. Instead, it introduces new energy levels (Fe^{3+}/Fe^{4+}) of the transition metal ions into the band gap of TiO_2. Therefore, the absorption edges shifting toward longer wavelengths for the Fe-doped TiO_2 should come from the electronic transition from the dopant energy level (Fe^{3+}/Fe^{4+}) to the conduction band of TiO_2. Additionally, Adán et al. [35] also states about the enhanced absorption in the visible region, which can be attributed to the excitation of 3d electrons of Fe^{3+} to the TiO_2 conduction band (charge transfer-transition) giving rise to a band centred at 400 nm. Besides, a band centered at ca. 500 nm, apparent for the samples with higher iron content, can be ascribed to the d-d transition of Fe^{3+} ($^2T_{2g} \rightarrow {}^2A_{2g}$, $^2T_{1g}$) or the charge transfer transition between interacting iron ions ($Fe^{3+} + Fe^{3+} \rightarrow Fe^{4+} + Fe^{2+}$).

The direct band gap energy for Fe-doped TiO_2 can be estimated from a plot of $(\alpha h\nu)^2$ versus photon energy ($h\nu$). The intercept of the tangent to the plot will give a good approximation of the band gap energy for Fe-doped TiO_2. According to Kormann et al. [37] and Rottenberger et al. [38], the absorption coefficient α can be calculated from the measured absorbance. The band gap energies estimated from the intercept of the tangents to the plots are 3.20, 2.97 and 2.88 eV for the doped metal concentrations at 0.0, 0.19 and 4.89 wt.%, respectively.

From Fig. 3, it is observed that $0.3FeTiO_2$ sample with low iron content shows a constant absorption in the visible region which is higher than $UTiO_2$. It can also be noticed that Fe doped TiO_2 powders have enhanced absorption characteristics in region of 450–650 nm, and this enhancement increases as the doped Fe is increased, accompanying with the change of powder color from primrose yellow to dark cream. It seems that photocatalytic activity under visible light depends on the addition of Fe.

Typical SEM images of $UTiO_2$, $0.3FeTiO_2$ and $7FeTiO_2$ powders are shown in Fig. 4. Shape of the particles is generally spherical and quite similar to each other. Spherical structure is become regular with increasing the doped Fe^{3+} concentration. However particle size distribution of the powders was not determined, the size of the particles varies in the range of 1.02–10.19 μm for $0.3FeTiO_2$, 1.06–9.89 μm for $7FeTiO_2$ and of 1.07–11.72 μm for $UTiO_2$, as measured using SEM images. Introducing Fe^{3+} ion decreased the particle size and gained more spherical shapes.

One interesting result obtained in this work is that the crystallite size and the particle size of the Fe^{3+} doped TiO_2 are smaller than those of $UTiO_2$, which can signify that the presence of Fe^{3+} in the reaction media might be used to control the particle and crystallite sizes of the oxides. Moreover, increasing the Fe^{3+} ion

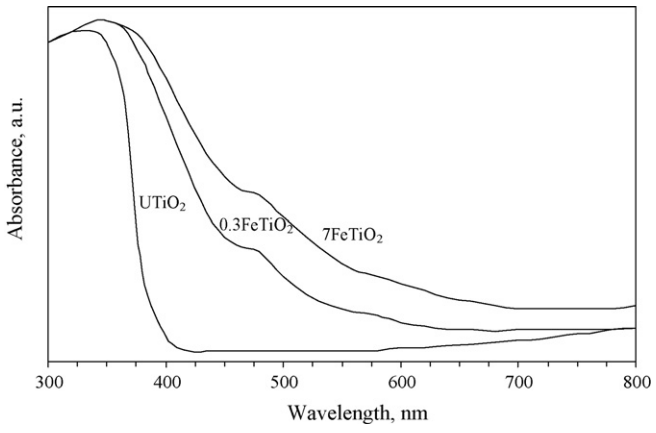

Fig. 3. UV–vis absorption spectrum of undoped and Fe doped-TiO_2 particles.

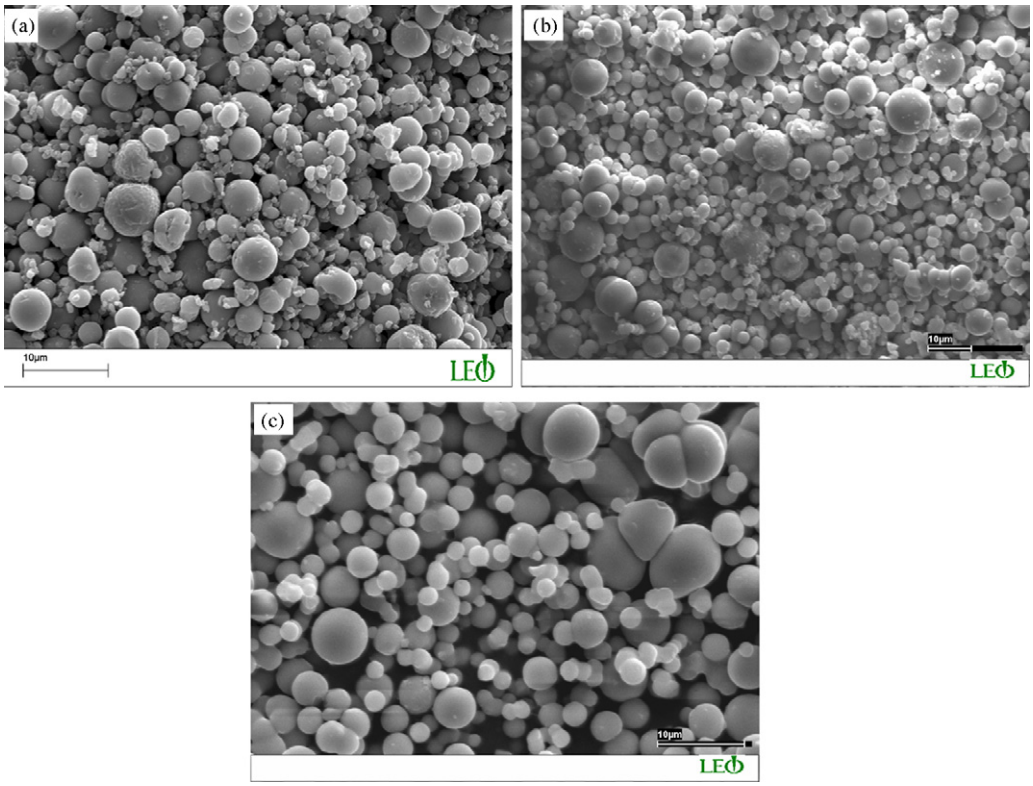

Fig. 4. SEM photomicrographs of (a) $UTiO_2$, (b) $0.3FeTiO_2$ and (c) $7FeTiO_2$ particles.

concentration decreases the particle size. Usually, the smaller the crystallite size, the larger the specific surface areas. Zhou et al. [39] also reported that the BET surface areas increased as Fe-doping concentration decreases. However, Fe-doped TiO_2 particles prepared by the sol–gel process is smaller than that of Degussa P25, but the BET surface area values of the particles are also smaller than that of Degussa P25. This is probably due to the fact that the long heat-treatment time of the samples at 773 K for 3 h and the heat of combustion of residual alkyls and organic substances cause the aggregation and sintering of the TiO_2 particles [40,41]. Leite et al. [42] also reported a novel approach to control particle size of Nb_2O_5 doped (5 mol%) SnO_2 prepared by the polymeric precursors method. They observed that Nb_2O_5–SnO_2 mixed oxide is formed with lower crystallite size than the pure SnO_2, with a Nb_2O_5–SnO_2 solid solution restricted to the surface of particles. The lower crystallite size of doped particles was attributed to this surface effect, with the Nb_2O_5 preventing the formation of necks between particles and the process of coalescence.

As expressed in Table 1, the film thickness was measured as 5, 6–8 and 5–7 μm for $UTiO_2$, $0.3FeTiO_2$ and $7FeTiO_2$ coated surfaces, respectively. Contact angle with water was measured as 60°, 69° and 65° on the original surfaces coated with $UTiO_2$, $0.3FeTiO_2$ and $7FeTiO_2$, respectively. After irradiation, it was measured as 17°, 8° and 7–8°, respectively. The decrease in the contact angle can be attributed to the reaction of produced electrons and holes in a different way. According to Fujishima et al. [11], the electrons tend to reduce the Ti(IV) cations to the Ti(III) state and the holes oxidizes the O^{2-} anions. In the process, oxygen atoms are rejected, creating oxygen vacancies. Water molecules can then occupy these oxygen vacancies, producing adsorbed OH groups which tend to make the surface hydrophilic, to form active OH radicals for further photocatalytic performance. Therefore, we can conclude that the irradiated surface has almost super-hydrophilic property and it has an important role for photocatalytic properties.

Photocatalytic activity test results for $0.3FeTiO_2$, $7FeTiO_2$ and $UTiO_2$ coated surfaces employed for degradation of MG under UV and vis-lights irradiation are shown in Figs. 5 and 6. It was observed that photocatalytic performance of Fe-doped TiO_2 thin films for the degradation of MG is higher than that of undoped TiO_2 films either under UV or vis-lights. Iron ion doping improves the photocatalytic activity. 75, 81 and 73%, and 58, 76 and 68% of initially 2.5 mg L^{-1} MG was degradated with $UTiO_2$, $0.3FeTiO_2$ and $7FeTiO_2$ thin films in 110 min under UV and vis-lights irradiation, respectively (Fig. 5). When initial concentration of MG was increased to 5.0 mg L^{-1}, 76%, 85% and 83%, and 64%, 77% and 79% of MG was degradated under UV and vis-lights irradiation (Fig. 6). It was revealed that the photodegradation rate increases with the increase in dye concentration under UV and vis-lights irradiation. Under the

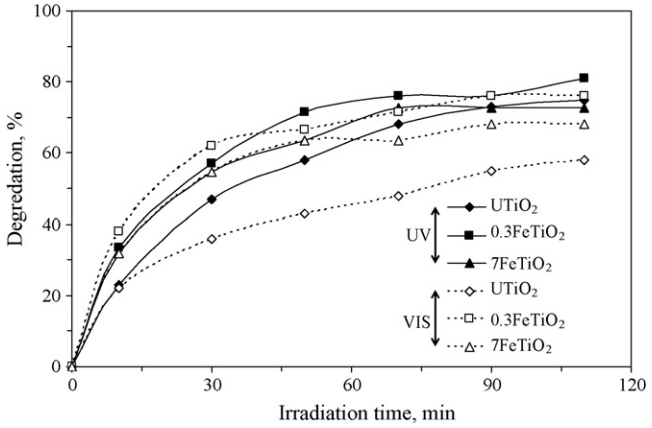

Fig. 5. Photocatalytic degradation of 2.5 mg L^{-1} MG under UV and vis-light irradiation.

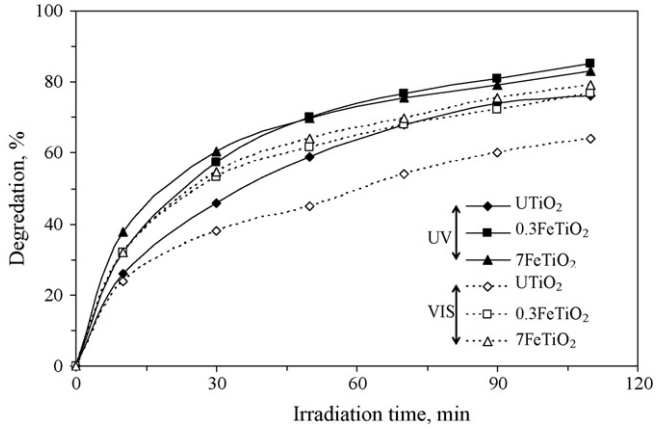

Fig. 6. Photocatalytic degradation of 5.0 mg L^{-1} MG under UV and vis-light irradiation.

same conditions, photoactivity of $UTiO_2$ thin film is less important than that of $0.3FeTiO_2$ and $7FeTiO_2$ thin films and $0.3FeTiO_2$ is more photoactive than $7FeTiO_2$. There are various reasons for the increase in the photocatalytic performance:

(a) High photocatalytic activity of Fe-doped TiO_2 may be related to small crystal size and high surface area as well as its mesoporous structure. It is well known that, as the particle size decreases, the surface area increases, and as the process is adsorption-dependent, the photocatalytic photodegradation rates also increases. Thus, $0.3FeTiO_2$ and $7FeTiO_2$ coated surfaces, which have surface areas of 83 and 126.1 $m^2\ g^{-1}$, respectively, showed that higher photocatalytic performance than $UTiO_2$, which has a surface area of 40.84 $m^2\ g^{-1}$ (Table 1). Dagan and Tomkiewicz [43] and Tomkiewicz et al. [44] also showed that TiO_2 with a surface area of 600 $m^2\ g^{-1}$ showed greater activity then commercial Degussa P-25 which has a surface area of 55 $m^2\ g^{-1}$. The effect of Fe^{3+} doping on the photocatalytic activity under UV light irradiation should be due to the reason that an appropriate amount of Fe^{3+} ions can act as intermediates for photo-generated holes and electrons transfer, and inhibit the recombination of holes and electrons.

Due to the facts that the energy level for Fe^{3+}/Fe^{4+} is above the valence band edge of TiO_2 and the energy level for Fe^{3+}/Fe^{2+} is below the conduction band edge of TiO_2 [45,46], Fe^{3+} ions, acting as both electrons and holes traps, can turn into Fe^{2+} and Fe^{4+} ions by trapping photogenerated electrons and holes traps, respectively Eqs. (1)–(4). According to the viewpoint of crystal field theory [47], Fe^{2+} and Fe^{4+} ions are relatively unstable when compared to Fe^{3+} ions, which have half-filled $3d^5$ orbital. Therefore, the trapped charges can easily release from Fe^{2+} or Fe^{4+} ions and then migrate to the surface to initiate the photocatalytic reaction. Fe^{2+} ions can be oxided to Fe^{3+} ions by transferring electrons to absorbed O_2 on the surface of TiO_2 Eq. (5) or a neighboring surface Ti^{4+} ions Eq. (6). Meanwhile, the adsorbed O_2 is reduced to O_2^- Eqs. (4) and (6), which can further degrade MG (Scheme 2). Similarly, Fe^{4+} ions also are reduced to Fe^{3+} ions by releasing electrons, while surface hydroxyl group translates into hydroxyl radical Eq. (7). As a result, the introduction of appropriate Fe^{3+} ions is responsible for the reduction of the photogenerated hole-electron recombination rate and favors the improvement of photocatalytic activity.

$$TiO_2 + h\nu \rightarrow e^- + h^+ \quad (1)$$

$$Fe^{3+} + h^+ \rightarrow Fe^{4+} \quad (2)$$

$$Fe^{3+} + e^- \rightarrow Fe^{2+} \quad (3)$$

$$Fe^{2+} + O_2(ads) \rightarrow Fe^{3+} + O^{2-} \quad (4)$$

$$Fe^{2+} + Ti^{4+} \rightarrow Fe^{3+} + Ti^{3+} \quad (5)$$

$$Ti^{3+} + O_2(ads) \rightarrow Ti^{4+} + O_2^- \quad (6)$$

$$Fe^{4+} + OH^-(ads) \rightarrow Fe^{3+} + OH^{\bullet}(ads) \quad (7)$$

However, when the concentration of Fe^{3+} ions becomes too large, Fe^{3+} ions can act as the recombination centers for the photo-generated electrons and holes Eqs. (1), (4) and (8)–(10), resulting in the decrease of photocatalytic activity.

$$Fe^{4+} + e^- \rightarrow Fe^{3+} \quad (8)$$

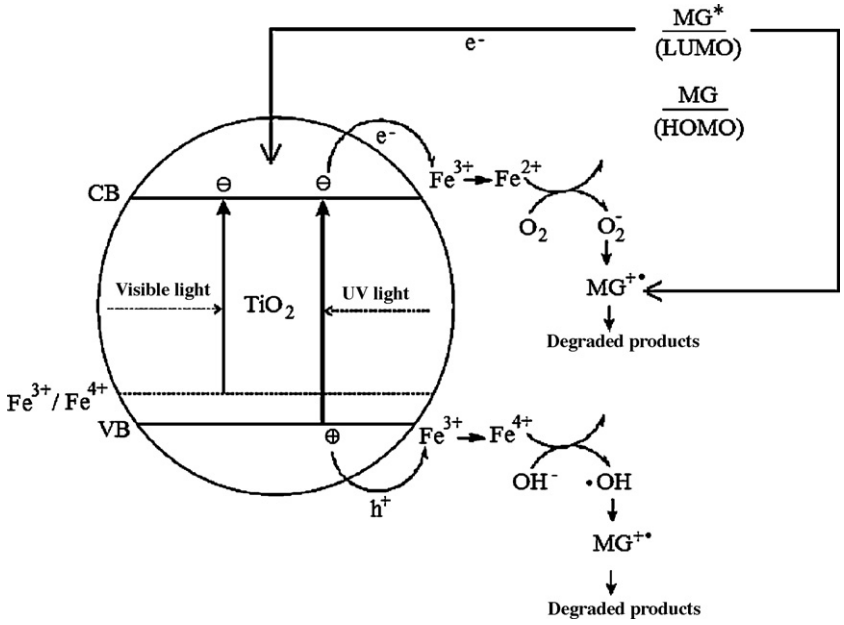

Scheme 2. Proposed mechanism for MG degradation under UV and vis-light irradiations.

$$Fe^{2+} + h^+ \rightarrow Fe^{3+} \quad (9)$$

$$Fe^{2+} + OH^\bullet \rightarrow Fe^{3+} + OH^- \quad (10)$$

Different with the intrinsic excitation of TiO_2 under UV irradiation, the excitation behavior of Fe–TiO_2 under visible irradiation arises from the electronic transition from the dopant energy level (Fe^{3+}/Fe^{4+}) to the conduction band of TiO_2. Due to the fact that the t_{2g} level of 3d orbital of Fe^{3+} ion is above the valence band of TiO_2, Fe^{3+} ion can absorb a photon with a wavelength exceeding 400 nm to produce a Fe^{4+} ion and a TiO_2 conductive band electron. The conductive band electron further reacts with adsorbed O_2 to form O_2^-, while Fe^{4+} reacts with surface hydroxyl group to produce hydroxyl radical. Furthermore, dopant Fe^{3+} improves electron transfer efficiency from the LUMO band of MG to the conduction band of Fe-doped TiO_2. Subsequently, increasing the amounts of radicals occurred above as shown in Scheme 2. Thus, MG was photodegraded even under the visible light irradiation [46] Eqs. (11)–(15).

$$Fe^{3+} + h\nu \rightarrow Fe^{4+} + e^- \quad (11)$$

$$e^- + O_2(ads) \rightarrow O_2^- \quad (12)$$

$$(TiO_2)e_{CB} + MG_{(LUMO)} \rightarrow (TiO_2)e^-{}_{CB} + MG^{+\bullet}{}_{(LUMO)} \quad (13)$$

$$MG^{+\bullet}{}_{(LUMO)} + O_2^- \rightarrow \text{“degraded products”} \quad (14)$$

$$MG^+ + HO^\bullet \rightarrow \text{“degraded products”} \quad (15)$$

(b) The increase in photocatalytic activity with Fe doping is related to shift in optical absorption of the catalyst in visible region. Pure TiO_2 absorbs only UV energy (≈380 nm) whereas Fe doped catalyst absorbs vis energy beside UV energy, hence there is increase in the photocatalytic activity.

(c) As dye concentration increases in solution, the photodegradation rate decreases. Briefly, the higher the concentration, the lower the rate of photodegradation. This negative effect can be commented as follows; as the dye concentration is increased, the equilibrium adsorption of dye on catalyst surface active sites increases, hence competitive adsorption of OH^- on the same sites decreases, which means a lower formation rate of $OH^\bullet$ radical which is the principal oxidant indispensable for a high photodegradation efficiency. When the dye concentration increases the amount of dye adsorbed on the catalyst surface increases. The increase in dye concentration also decreases the path length of photon entering the dye solution. At high dye concentration a significant amount of solar light may be absorbed by the dye Molecules rather than the catalyst and this may also reduce the catalytic efficiency. Consequently, the degradation efficiency of the dye decreases as the dye concentration increases.

(d) The high photocatalytic performance of the coated plate can also be related to its surface which has almost super hydrophilic property. These reasons are confirmed with the obtained results by Schmidt et al. [48].

Kinetics of the degradation was also investigated. However the regression coefficients for the degradation of 2.5 mg L^{-1} initial MG concentrations are low, it was determined that photocatalytic degradation of MG follows the pseudo-first-order reaction kinetics with a good agreement with the literature [49]. The pseudo-first-order reaction kinetics is represented by the following equation

$$\ln C_0 - \ln C = kt \quad (16)$$

where C is the final concentration (mg L^{-1}) of MG after irradiation, C_0 is the initial concentration (mg L^{-1}) of MG prior to irradiation, t is the irradiation time (min) and k is the apparent reaction rate constant (min^{-1}). For this reason, photocatalytic degradation data

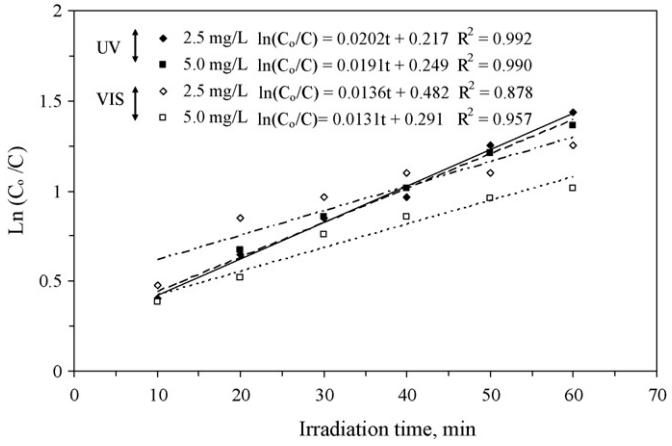

Fig. 7. Pseudo-first-order reaction kinetics curves for photocatalytic degradation of MG with 0.3FeTiO_2 catalyst under UV and vis-light irradiation.

presented in Figs. 5 and 6 for 0.3FeTiO_2 sample were re-plotted in the $\ln C_0/C - t$ coordinates (Fig. 7). It was observed that the values of rate constants, k, are consistent with the photodegradation of MG. For example, 81% and 85% of 2.5 and 5.0 mg L^{-1} MG, respectively, was degradated with 3FeTiO_2 thin film within 110 min with UV irradiation (Figs. 5 and 6). Photodegradation rate constants were determined as 0.0202 and 0.0191 min^{-1}, respectively. On the other hand, 76% and 79% of 2.5 and 5.0 mg L^{-1} MG, respectively, was degradated with 0.3FeTiO_2 under vis irradiation (Figs. 5 and 6). The rate constants are 0.0136 and 0.0131 min^{-1}, respectively.

4. Conclusions

Nano-sized Fe-doped and undoped TiO_2 particles were synthesized by hydrothermal process at low temperature. $Ti(OPr^i)_4$ was used as starting material. The particles were fully anatase crystal form, simply dispersed in water and they can be easily used to obtain thin films on different surfaces. In this work, very transparent, hydrophilic and smooth TiO_2-based thin films were prepared by spin-coating technique. Doping of the Fe^{3+} ion decreased the particle size which resulted in an increase in the surface area. The photocatalytic performance of Fe-doped TiO_2 thin film for degradation of MG was higher than that of the undoped TiO_2 film under UV and VIS lights. It was determined that degradation of MG with use of Fe^{3+} doped TiO_2 thin films follows the pseudo-first-order reaction kinetics. Use of Fe-doped TiO_2 coated surfaces for preparing self-cleaning and/or an antibacterial surface is suggested.

Acknowledgements

The authors gratefully acknowledge the financial support of TR Prime Ministry State. Planning Organization (Project number: 2005 DPT.120.150). They also thank Dr. Murat Erdemoğlu for his valuable comments during the preparation and revising procedure of the manuscript.

References

[1] A. Kumbhar, G. Chumanov, Synthesis of iron(III)-doped titania nanoparticles and its application for photodegradation of sulforhodamine-B pollutant, J. Nanopart. Res. 7 (2005) 489–498.
[2] W.Y. Zhou, S.Q. Tang, L. Wan, K. Wei, D.Y. Li, Preparation of nano-TiO_2 photocatalyst by hydrolyzation–precipitation method with metatitanic acid as the precursor, J. Mater. Sci. 39 (2004) 1139–1144.
[3] S.J. Hwang, C. Petucci, D. Raftery, In situ solid-state NMR studies of trichloroethylene photocatalysis: formation and characterization of surface-bound intermediates, J. Am. Chem. Soc. 120 (1998) 4388–4397.

[4] M. Andersson, L. Osterlund, S. Ljungström, A. Palmqvist, Preparation of nanosize anatase and rutile TiO_2 by hydrothermal treatment of microemulsions and their activity for photocatalytic wet oxidation of phenol, J. Phys. Chem. B 106 (41) (2002) 10674–10679.
[5] H. Tada, A. Hattori, Y. Tokihisa, K. Imai, N. Tohge, S. Ito, A patterned-TiO_2/SnO_2 bilayer type photocatalyst, J. Phys. Chem. B 104 (19) (2000) 4585–4587.
[6] M.R. Hoffman, S.T. Martin, W. Choi, D.W. Bahnemann, Environmental applications of semiconductor photocatalysis, Chem. Rev. 95 (1995) 69–96.
[7] Y. Ohko, A. Fujishima, K. Hashimoto, Kinetic analysis of the photocatalytic degradation of gas-phase 2-propanol under mass transport-limited conditions with a TiO_2 film photocatalyst, J. Phys. Chem. B 102 (1998) 1724–1726.
[8] J.M. Hermann, Heterogeneous photocatalysis: fundamentals and applications to the removal of various types of aqueous pollutants, Catal. Today 53 (1999) 115–129.
[9] Y. Cao, W. Yang, W. Zhang, G. Liu, P. Yue, Improved photocatalytic activity of Sn^{4+} doped TiO_2 nanoparticulate films prepared by plasma-enhanced chemical vapor deposition, New J. Chem. 28 (2004) 218–222.
[10] Q. Liu, X. Wu, B. Wang, Q. Liu, Preparation and super-hydrophilic properties of TiO_2/SnO_2 composite thin films, Mater. Res. Bull. 37 (2002) 2255–2262.
[11] A. Fujishima, T.N. Rao, D.A. Tryk, Titanium dioxide photocatalysis, J. Photochem. Photobiol. C: Photochem. Rev. 1 (2000) 1–4.
[12] V. Subramanian, E. Wolf, P.V. Kamat, Semiconductor-metal composite nanostructures. To what extent do metal nanoparticles improve the photocatalytic activity of TiO_2 films? J. Phys. Chem. B 105 (2001) 11439–11446.
[13] K. Rajeshwar, N.R. De Tacconi, C.R. Chenthamarakshan, Chem. Mater. B 13 (9) (2001) 2765–2782.
[14] C. Lettmann, H. Hinrichs, W.F. Maier, Combinatorial discovery of new photocatalysts for water purification with visible light, Angew. Chem. Int. Ed. 40 (2001) 3160–3163.
[15] K.T. Ranjit, B. Viswanathan, Photocatalytic properties of iron-doped titania semiconductors, J. Photochem. Photobiol. A: Chem. 108 (1997) 79–84.
[16] M.I. Litter, J.A. Navigo, Photocatalytic properties of iron-doped titania semiconductors, J. Photochem. Photobiol. A: Chem. 98 (3) (1996) 171–181.
[17] J.A. Navigo, G. Colon, M. Macias, C. ReL, M.I. Litter, Iron-doped titania semiconductor powders prepared by a sol–gel method. Part I: synthesis and characterization, Appl. Catal. A: Gen. 177 (1999) 111–120.
[18] Z. Zhang, C. Wang, R. Zakaria, J.Y. Ying, Role of particle size in nanocrystalline TiO_2-based photocatalysts, J. Phys. Chem. B 102 (1998) 10871–10878.
[19] M. Tomkiewicz, Scaling properties in photocatalysis, Catal. Today 58 (2000) 115–123.
[20] K. Mizushima, M. Tanaka, A. Asai, S. Lida, J. Goodenough, Impurity levels of iron-group ions in TiO_2, J. Phys. Chem. Solids 40 (12) (1979) 1129–1140.
[21] J.A. Navio, J.J. Testa, P. Djedjeian, J.R. Padron, D. Rodriguez, M.I. Litter, Iron-doped titania powders prepared by a sol–gel method: part II: photocatalytic properties, Appl. Catal. A: Gen. 178 (2) (1999) 191–203.
[22] O.M. Alfano, D. Bahnemann, A.E. Cassano, R. Dillert, R. Goslich, Photocatalysis in water environments using artificial and solar light, Catal. Today 58 (2/3) (2000) 199–230.
[23] W. Choi, A. Termin, M.R. Hoffmann, rThe Role of metal ion dopants in quantum-sized TiO_2: correlation between photoreactivity and charge carrier recombination dynamics, J. Phys. Chem. 98 (1994) 13669–13679.
[24] Y.F. Zhu, L. Zhang, L. Wang, Y. Fu, L.L. Gao, The preparation and chemical structure of TiO_2 film photocatalysts supported on stainless steel substrates via the sol–gel method, J. Mater. Chem. 11 (2001) 1864–1868.
[25] L. Zhang, Y. Zhu, Y. He, W. Li, H. Sun, Preparation and performances of mesoporous TiO_2 film photocatalyst supported on stainless steel, Appl. Catal. B: Environ. 40 (4) (2003) 287–292.
[26] G. Balasubramanian, D.D. Dionysiou, M.T. Suidan, Y. Subramanian, I. Baudin, J.M. Laine, Titania powder modified sol–gel process for photocatalytic applications, J. Mater. Sci. 38 (2003) 823–831.
[27] J.C. Yu, W.K. Ho, J. Lin, H. Yip, P.K. Wong, Photocatalytic activity, antibacterial effect, and photoinduced hydrophilicity of TiO_2 films coated on a stainless steel substrate, Environ. Sci. Technol. 37 (2003) 2296–2301.
[28] M. Kang, J.H. Lee, C.H. Chung, K.J. Yoon, K. Ogino, S. Miyata, S.J. Choung, Preparation of TiO_2 film by the MOCVD method and analysis for decomposition of trichloroethylene using in situ FT-IR spectroscopy, J. Mol. Catal. A Chem. 193 (2003) 273–283.
[29] W. Li, S.I. Shah, M. Sung, C.P. Huang, Structure and size distribution of TiO_2 nanoparticles deposited on stainless steel mesh, J. Vac. Sci. Technol. B 20 (6) (2002) 2303–2308.
[30] H. Sayılkan, Improved photocatalytic activity of Sn^{4+}-doped and undoped TiO_2 thin film coated stainless steel under UV- and vis-irradiation, Appl. Catal. A: Gen. 319 (2007) 230–235.
[31] P.H. McMurry, A review of atmospheric aerosol measurements, Atmos. Environ. 34 (2000) 1959–1999.
[32] J.G. Yu, X.J. Zhao, Effect of surface treatment on the photocatalytic activity and hydrophilic property of the sol–gel derived TiO_2 thin films, Mater. Res. Bull. 36 (1/2) (2001) 97–107.
[33] M. Akarsu, M. Asiltürk, F. Sayılkan, N. Kiraz, E. Arpaç, H. Sayılkan, A novel approach to the hydrothermal synthesis of anatase titania nanoparticles and the photocatalytic degradation of rhodamine B, Turk. J. Chem. 30 (3) (2006) 333–343.
[34] C.Y. Wang, C. Bottcher, D.W. Bahnemann, J.K. Dohrmann, A comparative study of nanometer sized Fe(III)-doped TiO_2 photocatalysts: synthesis, characterization and activity, J. Mater. Chem. 13 (9) (2003) 2322–2325.
[35] C. Adán, A. Bahamonde, M. Fernández-García, A. Martínez-Arias, Structure and activity of nanosized iron-doped anatase TiO_2 catalysts for phenol photocatalytic degredation, Appl. Catal. B: Environ. 72 (2007) 11–17.
[36] K. Nagaveni, M.S. Hegde, G. Madras, Structure and photocatalytic activity of $Ti_{1-x}M_xO_2 \pm$ delta (M=W, V, Ce, Zr, Fe, and Cu) synthesized by solution combustion method, J. Phys. Chem. B 108 (52) (2004) 20204–20212.
[37] C. Kormann, D.W. Bahnemann, M.R. Hoffmann, Preparation and characterization of quantum-size titanium-dioxide, J. Phys. Chem. 92 (18) (1988) 5196–5201.
[38] G. Rothenberger, J. MGser, M. Graetzel, N. Serpone, D.K. Sharma, Charge carrier trapping and recombination dynamics in small semiconductor particles, J. Am. Chem. Soc. 107 (26) (1985) 8054–8059.
[39] M. Zhou, J. Yu, B. Cheng, H. Yu, Preparation and photocatalytic activity of Fe-doped mesoporous titanium dioxide nanocrystalline photocatalysts, Chem. Phys. 93 (2005) 159–163.
[40] G. Yu, H.G. Yu, B. Cheng, X.J. Zhao, J.C. Yu, W.K. Ho, The effect of calcination temperature on the surface microstructure and photocatalytic activity of TiO_2 thin films prepared by liquid phase deposition, J. Phys. Chem. B 107 (2003) 13871–13879.
[41] J.G. Yu, J.C. Yu, M.K.P. Leung, W.K. Ho, B. Cheng, X.J. Zhao, J.C. Zhao, Effects of acidic and basic hydrolysis catalysts on the photocatalytic activity and microstructures of bimodal mesoporous titania, J. Catal. 217 (2003) 69–78.
[42] E.R. Leite, I.T. Weber, E. Longo, J.A. Varela, A new method to control particle size and particle size distribution of SnO_2 nanoparticles for gas sensor applications, Adv. Mater. 12 (2000) 965–968.
[43] G. Dagan, M. Tomkiewicz, TiO_2 aerogels for photocatalytic decontamination of aquatic envıronments, J. Phys. Chem. 97 (49) (1993) 12651–12655.
[44] M. Tomkiewicz, G. Dagan, Z. Zhu, Morphology and photocatalytic activity of TiO_2 aerogels, Res. Chem. Intermed. 20 (7) (1994) 701–710.
[45] Y. Ma, X.T. Zhang, Z.S. Guan, Y.A. Cao, J.N. Yao, Effects of zinc(II) and iron(III) doping of titania films on their photoreactivity to decompose rhodamine B, J. Mater. Res. 16 (10) (2001) 2928–2933.
[46] T. Tong, J. Zhang, B. Tian, F. Chen, D. He, Preparation of Fe^{3+}-doped TiO_2 catalysts by controlled hydrolysis of titanium alkoxide and study on their photocatalytic activity for methyl orange degradation, J. Hazard. Mater. 155 (3) (2008) 572–579.
[47] M.H. Zhou, J.G. Yu, B. Cheng, Effects of Fe-doping on the photocatalytic activity of mesoporous TiO_2 powders prepared by an ultrasonic method, J. Hazard. Mater. 137 (3) (2006) 1838–1847.
[48] H. Schmidt, M. Akarsu, T.S. Muller, K. MGh, G. Schafer, D.J. Strauss, M. Naumann, The formation of gradients in wet deposited coatings with photocatalytically active anoparticles, Res. Chem. Intermed. 31 (4–6) (2005) 535–538.
[49] F. Sayılkan, M. Asiltürk, P. Tatar, N. Kiraz, Ş. Şener, E. Arpaç, H. Sayılkan, Photocatalytic performance of Sn-doped TiO_2 nanostructured thin films for photocatalytic degradation of malachite green dye under UV and vis-lights, Mater. Res. Bull. 43 (2008) 127–134.